HIGH-TEMPERATURE OXIDATION BEHAVIOR OF KANTHAL APM AND D ALLOYS IN STEAM

Chongchong Tang [a]*, Martin Steinbrueck [a], Mirco Grosse [a], Adrian Jianu [b], Alfons Weisenburger [b], Hans Juergen Seifert [a]

[a]Karlsruhe Institute of Technology, Institute for Applied Materials
[b]Karlsruhe Institute of Technology, Institute for Pulsed Power and Microwave Technology
PO Box 3640, 76021 Karlsruhe, Germany
Chongchong.tang@kit.edu

The oxidation behavior of two commercial FeCrAl alloys, Kanthal APM and D, with high Cr content (20.5 wt.% Cr, 4.8-5.8 wt.% Al) was investigated under well-defined heating schedules at 1300-1500°C in steam. In isothermal tests, both alloys melted at 1500°C, rapidly and completely oxidized at 1400°C, and formed protective alumina scales at 1300°C. Ramp tests starting from 500°C were conducted with two different heating rates: 5 and 10 K/min. Complete oxidation of both alloys was observed at 10 K/min below 1400°C, and the maximum tolerant temperatures of APM and D (determined by hydrogen release rate) were only 1379°C and 1374°C, respectively. Protective α-Al$_2$O$_3$ scales formed on all alloys at 5 K/min or pre-oxidation at lower temperature (1200°C for 1 hour) which can provide protection up to the melting temperature. Transient oxide layers with high concentration of Fe and Cr were observed and the maximum tolerance temperature of FeCrAl alloys in steam was significantly determined by the Al content, Al diffusion rate in the bulk material and the heating schedules adopted.

I. INTRODUCTION

The attractive properties of zirconium alloys, including low neutron absorption cross section, good corrosion performance, high strength and creep resistance in hot water, promoted the selection and development of them for use as nuclear fuel cladding and structural components in water cooled nuclear reactors[1]. However, the exothermic reaction between Zircaloy cladding and steam during beyond design-basis nuclear reactor accident (BDBA) scenarios that can accelerate the raise of the core temperature to such high level that the cladding, fuel and core structures are at risk of melting. It is problematic because the temperature escalation is accompanied by a rapid hydrogen production due to the zirconium-steam reaction. Hydrogen detonation can occur associated by release of highly-radioactive fission products, as it happened in the Fukushima nuclear reactor accident[2,3].

Post Fukushima, the possibility of replacing current Zr-based alloys by so called accident-tolerant fuel (ATF) claddings is being investigated[4]. These materials should provide improved oxidation kinetics with steam and, hence, larger safety margins.

Different categories of ATF cladding materials, including metals (like ODS steel, FeCrAl alloys) and ceramics (like SiC, $M_{n+1}AX_n$ phases) have been proposed as candidate accident-tolerant fuel cladding materials[5,6]. One of the challenging properties that must be optimized before ceramics can be used as candidate cladding materials is their inherently brittle nature[7,8]. FeCrAl-based alloys attract a lot of attention and seem to be the most promising candidate for near term solution due to their excellent properties, like formability, high mechanical properties and high temperature oxidation resistance[9–12]. Traditional FeCrAl alloys with relative high chromium addition (~20 wt.%) aim at high-temperature oxidizing applications, e.g. heating elements and catalytic converters[13]. For nuclear application, formation of the Cr-rich α' phase under irradiation causes significant radiation-induced hardening and embrittlement for traditional high-Cr alloys[9,14,15]. Current research and development efforts of nuclear grade alloys have focused on balancing the chromium and aluminum content to lower chromium concentrations[12,16,17].

The high-temperature oxidation resistance of FeCrAl alloys relies on the formation of a slow-growing, adherent, and stable alumina scale on the surface. The addition of around 20 wt.% Cr reduces the amount of Al needed to establish the protective alumina scale[18]. It is generally believed that transient aluminas, γ-, δ- and θ-Al$_2$O$_3$, formed at lower temperature (below 950°C) and the transient aluminas convert to α-Al$_2$O$_3$ which has dense structure and provides better protection at elevated temperature[19–21]. Further studies have demonstrated that steam pressure and the existence of hydrogen have little effects on the oxidation kinetics of alumina-forming materials[17,22]. Even though intensive studies have been conducted to investigate the oxidation behavior of FeCrAl alloys in steam, the test temperatures were relative low

(< 1300°C). The focus was placed on steady-state oxidation[13,17,23]. Few studies in the literature have been found with temperature up to 1400°C in steam. The knowledge of the influence of alloy composition and heating rate on the successful establishment of protective alumina scale at elevated temperature is not yet satisfying[12].

Therefore, this study focused on the influence of heating schedules on the oxidation behavior of two commercial alloys, Kanthal APM and D with high Cr content and different Al concentration, in steam in the temperature range 1300-1500°C. The oxidation kinetics was recorded via the hydrogen release and the failure mechanism was analyzed from the thermodynamic view.

II. EXPERIMENT

Kanthal APM and D tubes were purchased from Kanthal/Sandvik, Sweden. The chemical compositions of these two alloys are shown in Table 1 given in wt.%. 0.5% ZrO_2-oxide is dispersed in both alloys. The main difference between these two alloys is the Al content, which is one percent higher of APM than that of D. Tube specimens for oxidation experiments were cut from a long tube by conventional band saw. The specimens are around 4 mm long for both alloys, but the outer diameter (APM: 25 mm, D: 6.0 mm) and the wall thickness (APM: 1.6 mm, D: 0.4 mm) are different. The cutting ends were deburred and ground to 1200 grit with SiC paper. Then the specimens were washed in ultrasonic solution with the sequence of 10 min deionized water, 10 min isopropanol, finally dried in hot air.

TABLE I. Alloy chemical compositions (wt.%)

Alloy	Cr	Al	C	Si	Mn	ZrO_2	Fe
APM	20.5	5.8	0.04	0.3	0.2	0.5	Bal.
D	20.5	4.8	0.04	0.3	0.2	0.5	Bal.

All the oxidation experiments in this study were conducted using a horizontal corundum tube furnace under normal pressure. The specimen was laid on a corundum crucible sample holder which was placed at the center of furnace. The furnace temperature was controlled by a mantled thermocouple located in the upper part of the furnace tube. The gas atmospheres were defined by a Bronkhorst® flow controller and gas mixer. The composition of the off-gas was *in-suit* analyzed by a mass spectrometer Balzers GAM300 with accuracy up to 1 ppm. Pure steam atmosphere cannot be achieved because argon is needed to act as the carrier gas and also the reference gas for mass spectrometer analysis.

Two different kinds of tests were conducted, isothermal tests and ramp tests. In the isothermal tests, samples were heated in high purity Ar atmosphere (99.9999%) to the desired temperature (1300, 1400, 1500°C) with fixed heating rate 10 K/min and a gas flow rate of 40 l/h Ar. Then the atmosphere was changed to 20 l/h Ar and 20 g/h H_2O and held for different times. Finally, the samples were cooled down to room temperature in the furnace to room temperature in high purity Ar atmosphere with a gas flow rate of 40 l/h Ar. In the ramp tests, the steam was induced into the furnace at 500°C. The other parameters remain the same except two heating rates were adopted, 5 and 10 K/min. The concentration of the steam during oxidation was ~52 vol%. Fig. 1 illustrates the typical heating and gas flow rate history of the isothermal tests and the ramp tests. Another pre-oxidation test at 1200°C was also conducted to examine the effect of pre-oxidation on the early stage oxidation behavior in steam.

The mass of all specimens before and after oxidation was measured using an analytical balance with resolution of 0.0001 g. The surface phase compositions of the oxidized samples were characterized using X-ray diffraction (XRD, Seifert PAD II) with Cu Kα1 radiation (λ=0.154 nm) in Bragg–Brentano geometry (θ-2θ), a step size of 0.002 ° and a scan speed at 1 °/min. The surface and cross section microstructures were determined using a field-emission scanning electron microscope (SEM, Jeol JSM 800), equipped with energy-dispersive X-ray spectroscopy (EDX) for element analysis.
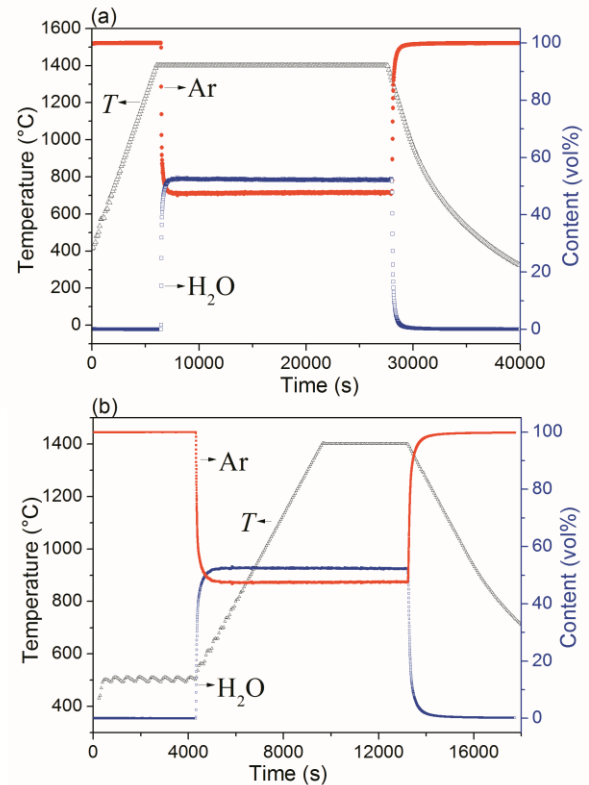
Fig. 1. Typical heating and gas flow rate history during oxidation tests in steam (a) isothermal test, (b) ramp test with 10 K/min heating rate.

III. RESULTS

III. A. Isothermal oxidation at 1300, 1400, 1500 °C in steam
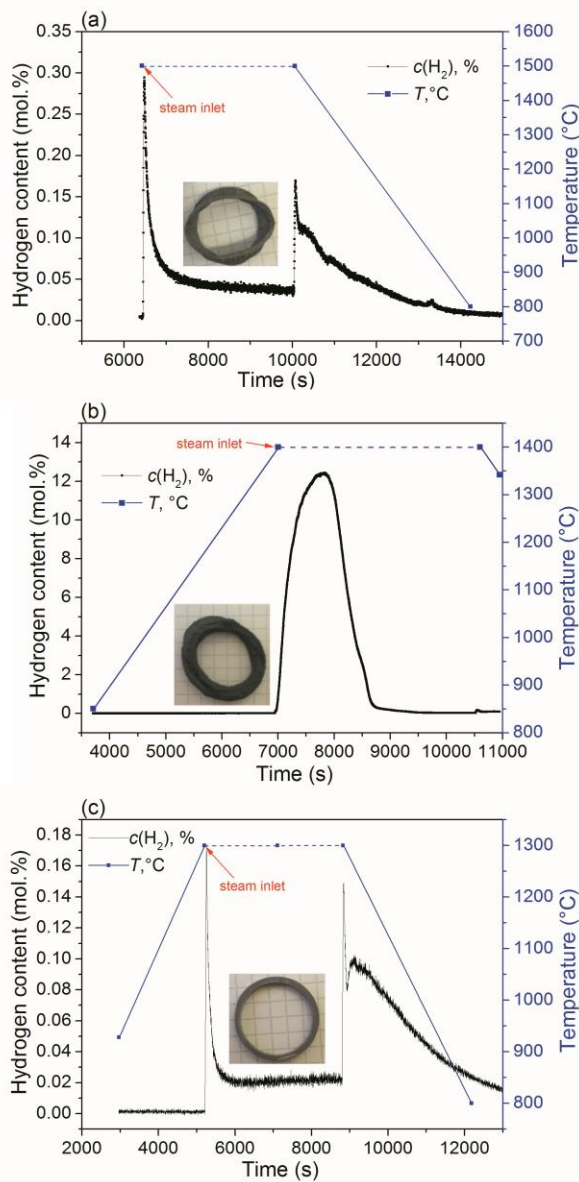
Fig. 2. Hydrogen release rates during oxidation with inserted sample appearance after oxidation of APM specimens in isothermal test (a) 1500°C, (b) 1400°C, (c) 1300°C. The grid in the appearance picture is 5 mm.

The oxidation rate is usually recorded as a function of mass gain of the specimen or the thickness of the oxide scale, but it also can be reflected *in-suit* by the hydrogen release during steam oxidation test. It can be especially meaningful to analysis the hydrogen release data when the mass gain cannot be *in-situ* measured at high temperature. Fig. 2 illustrates the hydrogen release rates during oxidation in isothermal tests for 1 h at three different temperatures of APM specimens. The inserted pictures show the appearance of the specimens after oxidation. Different behaviors were observed at these three temperatures. At 1500°C as shown in Fig. 2 (a), the sample partially melted and could not maintain its geometry. The two peaks shown in the hydrogen release rate curve were attributed to the change of the atmosphere in the furnace. The hydrogen content was relatively low and decreased gradually in the isothermal oxidation period. However, at 1400°C (Fig. 2 (b)), distinct behavior appeared. The color of the appearance transferred to deep dark and the structure of the sample became loose with grooves and pores. The hydrogen content increased sharply to a significantly higher level, more than one magnitude higher than that at 1500°C, and then decreased quickly to the level during heating up period. After examining the mass change of the sample, it can be concluded that the sample was rapidly and completely oxidized. An isothermal test for just 15 min was also conducted at 1400°C to verify this finding. The same behavior was observed. At 1300°C, the sample kept its shape and the hydrogen release rate was at the same order of magnitude as at 1500°C, but a little lower. The mass gains per unit area for samples oxidized at 1500°C and 1300°C were 1.21 mg/cm^2 and 0.33 mg/cm^2, respectively. The mass gains were consistent with the hydrogen release rates, indicating low oxidation rate. The Kanthal D specimens with low Al content showed similar behavior in the isothermal tests except the mass gain at 1500°C and 1300°C was slightly higher.
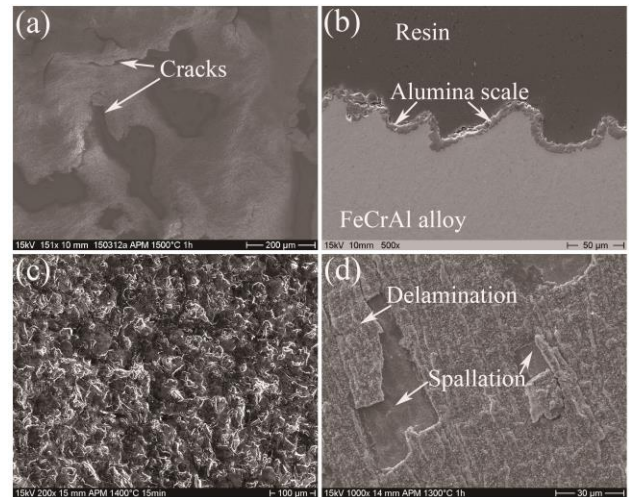
Fig. 3. Secondary electron images of typical surface and cross section morphologies of APM after isothermal oxidation at different temperatures (a) 1 h at 1500°C surface, (b) 1 h at 1500°C cross section, (c) 15 min at 1400°C surface, (c) 1 h at 1300°C surface.

Fig. 3 shows the surface and cross section morphologies of the APM alloy samples isothermally

oxidized at 1500-1300°C in steam. At 1500°C, the surface of the sample became rough due to deformation of the sample, but protective alumina scale formed on the surface as shown in Fig. 3 (a) and (b). The scale cracked due to concentrations of stress induced by the change of shape. A different morphology develops at the completely oxidized sample at 1400°C in steam for 15 min (Fig. 3 (c)). The surface structure became loose, apparently without formation of protective oxide scale. As can be seen from Fig. 3 (d), protective oxide scale formed for the sample oxidized at 1300°C in steam for 1 h, but the scale showed low adherence with delamination and spallation.

III. B. Ramp oxidation with 10 and 5 K/min heating rates in steam
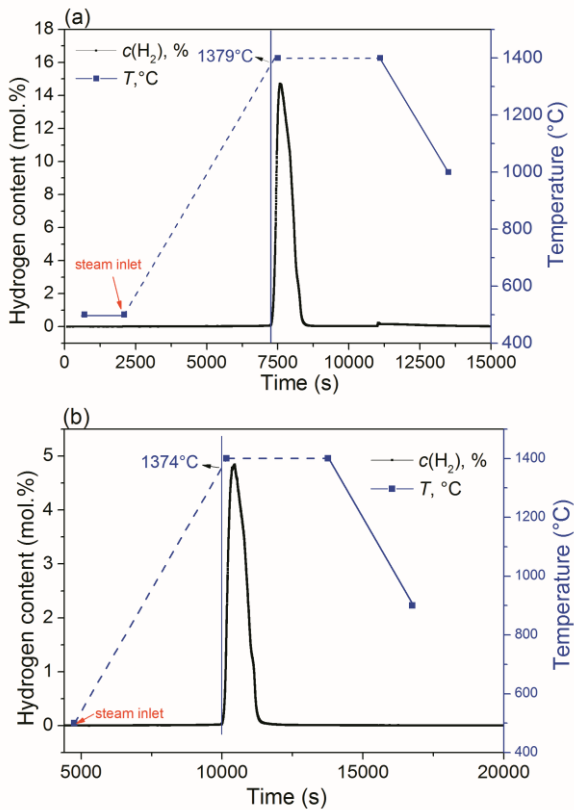
Fig. 4. Hydrogen release rates during 1400°C ramp tests with 10 K/min heating rate (a) APM sample, (b) D sample.

Ramp tests with two different heating rates were conducted to investigate the early stage oxidation behavior and determine the maximum tolerance temperature in steam. Fig. 4 shows the hydrogen release rates for both alloys with 10 K/min heating rate. Surprisingly, both alloys failed, i.e. rapid and complete consumption occurred like in the isothermal test at 1400°C, before the temperature reached 1400°C. The maximum tolerance temperature in steam determined by

hydrogen release was 1379°C for APM; for D with lower aluminum content it was 1374°C.

By decreasing the heating rate to 5 K/min, no rapid rise of the hydrogen release was observed whether the sample was heated to 1500°C or to 1400°C with 1 h holding time as shown in Fig. 5. The hydrogen release rate increased gradually with the rise of temperature except at around 960°C it decreased slightly to reach a peak (A) in Fig. 5 (a). This behavior was attributed to the transformation of metastable Al_2O_3 formed at low temperature to dense α-Al_2O_3 scale[20]. During the holding time at 1400°C, the hydrogen release rate decreased gradually. It indicates that a protective scale formed on the surface and the diffusion in the oxide scale became the controlling step.
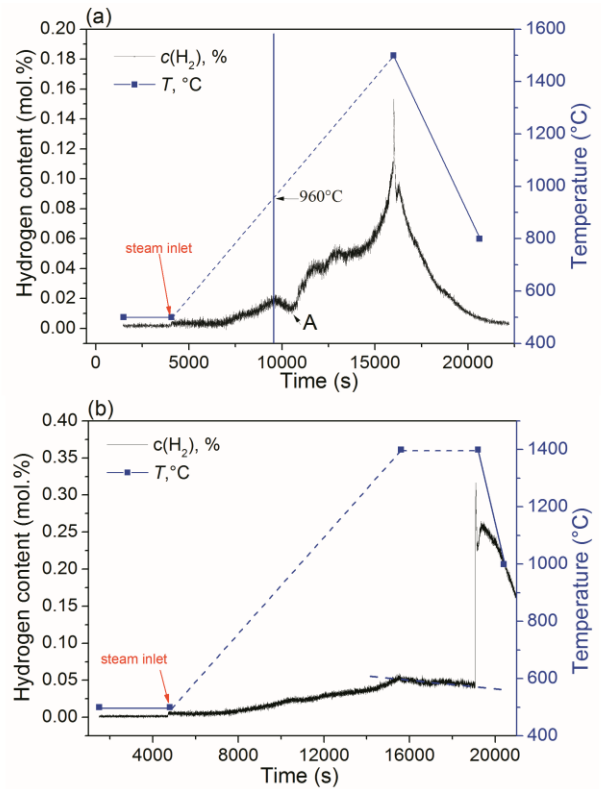
Fig. 5. Hydrogen release rates during ramp tests with 5 K/min heating rate of APM sample (a) no holding time at 1500°C, (b) 1 hour at 1400°C.

A pre-oxidation test was undertaken to examine its beneficial effect to improve the maximum tolerance temperature of the alloys in steam. Fig. 6 shows the hydrogen release rates by pre-oxidation at 1200°C for 1 h, then heated to 1400°C with 1 hour holding time. As seen from the picture, the hydrogen release rate maintained within a low level during the whole oxidation process, indicating that a protective scale formed. It is essential to illustrate that the hydrogen release rate remained constant during the holding time at 1200°C, however, decreased

gradually during the holding time at 1400°C, as shown in Fig. 6 by the dotted lines. This suggests that the oxidation kinetics follow a linear law at the early stage of oxidation before a continuously protective oxide was established. After it the kinetics was transferred to a parabolic or sub-parabolic law.
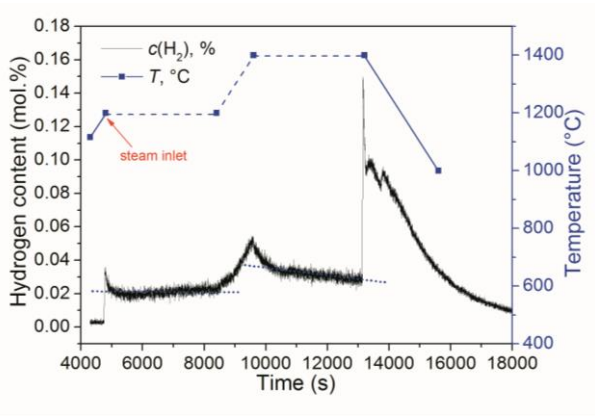
Fig. 6. Hydrogen release rate during ramp test of APM sample by pre-oxidation at 1200°C for 1 hour with 10 K/min heating rate.

Fig. 7 shows the oxidation kinetics of APM and D heated to 1400°C with 5 K/min heating rate and subsequent isothermal oxidation up to 10 hours, together with the mass gain by pre-oxidation at 1200°C for 1 h. For both alloys, the oxidation kinetics followed a sub-parabolic law. The oxidation rate of Kanthal D with low Al content was slightly higher than the rate of Kanthal APM. Pre-oxidation at 1200°C for 1 h had the similar effect as using the low heating rate of 5 K/min because the mass gains were similar.
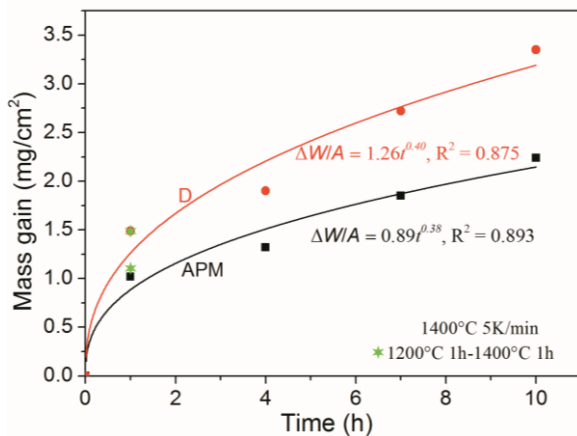
Fig. 7. Mass gain per unit surface area as a function of time for APM and D heated to 1400°C with 5 K/min heating rate and subsequent isothermal oxidation up to 10 hours in ramp tests. The solid lines indicate fitting relationship between the mass gain and oxidation time up to 10 hours.

The phase composition for APM and D samples heated to 1400°C with 5 K/min heating rate (subsequent 10 h isothermal oxidation) and with 10 K/min heating rate (subsequent 1 h isothermal oxidation) in steam after the ramp tests are shown in Fig. 8. The results further confirmed that protective α-Al_2O_3 scales formed on the surface with 5 K/min heating rate. For the samples which completely oxidized with 10 K/min heating rate, they were ground into powder for XRD measurement. The samples totally converted to the oxide of iron, chromium and aluminum, $Fe(Cr, Al)_2O_4$ and Fe_2O_3.
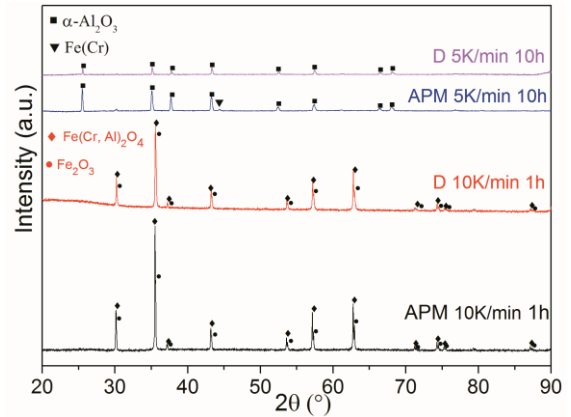
Fig. 8. X-ray diffraction patterns of the samples after oxidation in the ramp test with different heating rates and holding time.
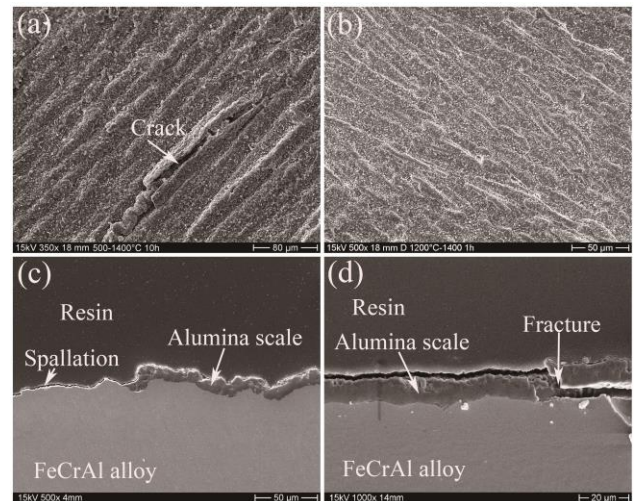
Fig. 9. Secondary electron images of the surface and cross section morphologies (a) Kanthal D 10 h at 1400°C ramp oxidation, (b) Kanthal D pre-oxidation at 1200°C for 1 h, then 1400°C for 1 h with 10 K/min heating rate, (c) Kanthal APM 10 h at 1400°C ramp oxidation, (d) Kanthal D 10 h at 1400°C ramp oxidation. The heating rates in the ramp tests were 5 K/min.

Fig. 9 (a) and (b) shows typical surface appearances of Kanthal D after ramp oxidation with 5 K/min heating

rate at 1400°C for 10 h and pre-oxidation at 1200°C for 1 h, then heated to1400°C for 1 h with 10 K/min heating rate. The surfaces looked similar and became coarse with formation of protective scale on the surface. Cracks and partial detachment of the scale were observed with prolonged oxidation time as shown in Fig. 9 (a). The cross section morphologies of Kanthal APM and D after 10 h oxidation in ramp tests were shown in Fig. 9 (c) and (d), respectively. The scale formed on APM showed lower adherence than that on D as partial spallation of the scale was observed for APM sample. No spallation but fracture and delamination of the scale was shown on the surface of D sample.

IV. DISCUSSION

It has been demonstrated that a critical Al and Cr content in FeCrAl alloys is needed to promote the formation of protective alumina scale during high-temperature oxidation at various temperature[18,24]. Important observations in this study affirm that heating schedules also have a profound effect on successful establishment of protective alumina scale. Both Kanthal APM and D alloys were completely oxidized at 1400°C in isothermal tests and below 1400°C in ramp tests with 10 K/min heating rate. Otherwise, protective alumina scales formed on the surface at 1500°C in isothermal test regardless of melting and at 1400°C in ramp tests with 5 K/min heating rate or after pre-oxidation at 1200°C for 1 h. Fig. 10 shows a scheme of the cross-sectional reaction and transport processes involved in the growth of oxide scale during oxidation[25]. The overall oxidation process can be divided into five main steps and the oxidation rates can be controlled by the gas phase mass transfer from the ambient to the surface, diffusion in the oxide and solid-mass transfer from the bulk to the interface. For FeCrAl alloys, most previous studies focused on the steady stage of oxidation, which means the protective scale has formed on the surface and the oxidation kinetics is usually controlled by the diffusion in the oxide scale, so the partial pressure of the oxidant (P'_{oxi}) at the substrate/oxide interface is very low. Based on the Ellingham diagram, alumina is the most stable oxide. The selective oxidation of aluminum during steady stage oxidation results in the growth of an alumina scale. However, at the early stage of oxidation before establishing of a continuous and protective alumina scale, the oxidation rate and the controlling step should be re-evaluated.

Transition oxidation stage was observed for alumina-forming materials during high temperature oxidation. Transient oxide layers formed during this stage usually containing more elements from the bulk material, like Fe and Cr from FeCrAl alloys[13,18,26]. Consequently, this oxide layer usually has loose structure and the oxidation kinetics is much faster, following a linear law during the transition oxidation stage. Fig. 11 displays the cross section view (BSE) and EDX line scan of Kanthal D after oxidation at 1400°C for 10 h in the ramp test with 5 K/min heating rate. A slightly brighter layer with dispersed white particles was shown on the surface. The EDX measurement detected that this layer contains high concentrations of Fe and Cr as shown in Fig. 11 (b) (region between the two dashed lines). The white particles are dispersed ZrO_2. Fig. 2 (c) and Fig. 6 (1200°C pre-oxidation period) demonstrate that the hydrogen release rates remain constant. This confirms the linear oxidation rate at the early stage of oxidation. Both findings prove that the transient oxide layer containing high content of elements from the bulk material induced by the transition stage. The oxidant can easily diffuse through this transition oxide layer and the partial pressure at the transient oxide layer/substrate interface is relative high as shown in Fig. 10 (P''_{tran}). If the sample can provide enough Al to consume the oxidant, a protective alumina scale is formed. If not, the transient oxide layer growth is continued until complete consumption of the sample. Moreover, the steam becomes more aggressive and diffuses faster with increasing temperature. This explains that a protective scale forms at 1300°C, but the samples fail and are completely oxidized at 1400°C. However, the diffusion of the Al in the substrate transfers from solid diffusion at 1400°C to liquid diffusion at 1500°C, which is significantly faster. Therefore, a protective alumina scale can form for the melted samples at 1500°C.
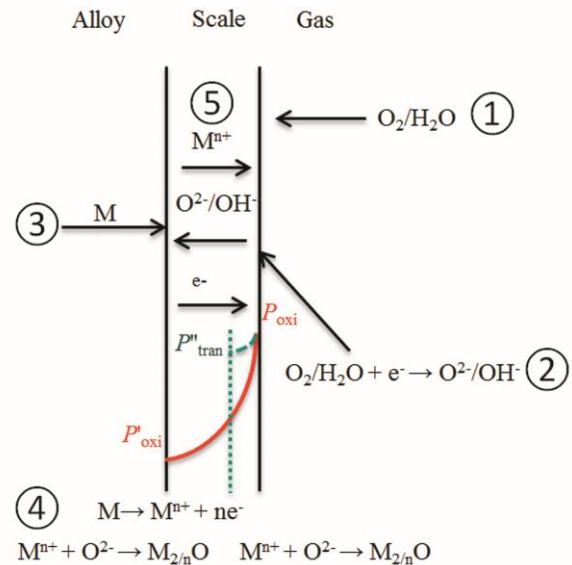
Fig. 10. Schematic cross-sectional view of reaction and transport processes involved in the growth of oxide scale during oxidation[25] (1) delivery of oxidant to the scale/gas interface via gas mass transfer, (2) incorporation of oxidant into the oxide scale, (3) delivery of reacting metal from the alloy to the alloy/scale interface, (4)

incorporation of metal into the oxide scale, (5) transport of metal and/or oxidant through the scale. The solid curve and the dash curve represent the depth profile of partial pressure of oxidant through the protective oxide layer and non-protective transient oxide layer, respectively.
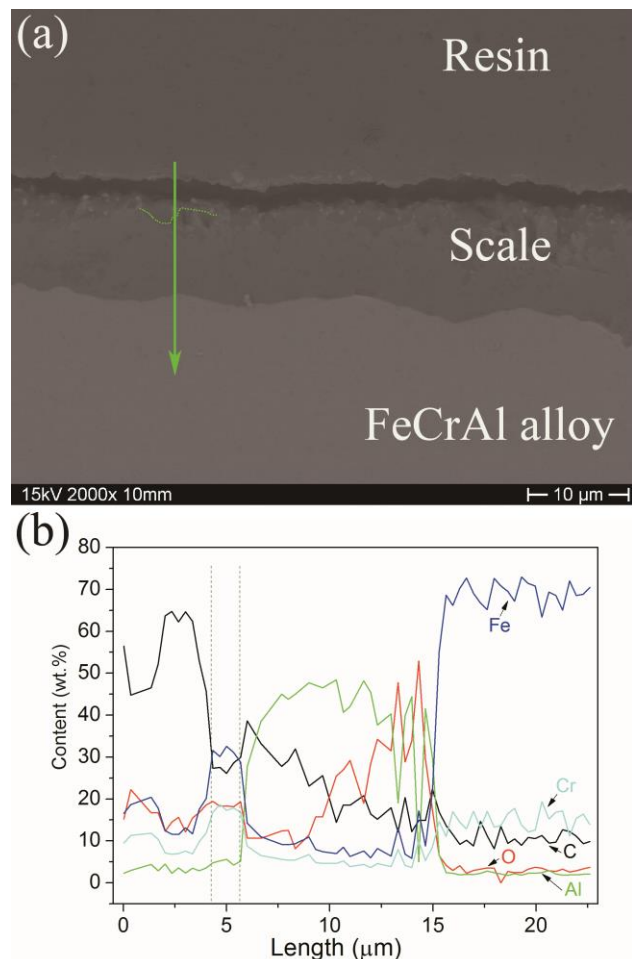
Fig. 11. Back scattered electron image of the cross section (a) and EDX line scan (b) of Kanthal D after oxidation at 1400°C for 10 hours in ramp test with 5 K/min heating rate.

The samples which are pre-oxidized with higher heating rate (10 K/min) fail below 1400°C but form a protective layer up to melting with 5 K/min heating rate or with pre-oxidation at 1200°C for 1 h. The reasonable explanation is that a continuous and thick enough alumina layer is needed to restrain the diffusion of the oxidant and to low the partial pressure at the substrate and scale interface to only oxidize the Al before the temperature reaching a high level. The maximum tolerance temperature is significantly influenced by the Al content in the bulk material and heating schedule adopted. For Kanthal APM with 1 percent higher content of Al than that of Kanthal D, the maximum tolerance temperature is 1379°C, 5 K higher than that of D. The oxidation rate is also slight lower after formation of a protective alumina scale. Due to this study focused on the early stage of oxidation and the oxidation time was relative short, the specimen thickness was supposed to have little effect on the oxidation behavior[27,28]. By increasing the Al content or pre-oxidation at lower temperature, the maximum tolerance temperature of FeCrAl alloys can be improved. More work need to be conducted for fully understanding the influence of Al and Cr content and the structure of the oxide formed at the early stage of oxidation on the maximum tolerance temperature of FeCrAl alloys in steam.

V. CONCLUSIONS

The oxidation behavior of two commercial FeCrAl alloys, Kanthal APM and D, was investigated at 1300-1500°C in steam. This work demonstrates that the heating schedules significantly affect the successful establishing of protective alumina scale at the early stage of oxidation. In isothermal tests, both alloys melted at 1500°C, rapidly and completely oxidized at 1400°C, and formed protective alumina scales at 1300°C. Ramp tests starting from 500°C were conducted with two different heating rates: 5 and 10 K/min. Complete oxidation of both alloys was observed at 10 K/min below 1400°C, and the maximum tolerance temperatures of APM and D were only 1379°C and 1374°C, respectively. Protective α-Al_2O_3 scales formed on all alloys during pre-oxidation at 5 K/min or at lower temperature (1200°C for 1 h) which can provide protection up to the melting temperature. The oxidation kinetics followed sub-parabolic law for both alloys after formation of protective alumina scale at 1400°C in steam with exposure time up to 10 hours. The APM alloy with higher Al content showed a lower oxidation rate. Transient oxide layer might be responsible for the catastrophic oxidation behavior observed at elevated temperature in case of samples heated with 10 K/min . The maximum tolerance temperature for FeCrAl alloys in steam was significantly determined by the Al content, Al diffusion rate in the bulk material and the heating schedules adopted. Increasing the Al content or pre-oxidation to obtain sufficient thick alumina scale can increase the maximum temperature capability of FeCrAl alloys in steam.

REFERENCES

1. B. COX, J. Nucl. Mater. **336**, 331 (2005).
2. M. STEINBRUECK, M. GROSSE, L. SEPOLD, and J. STUCKERT, Nucl. Eng. Des. **240**, 1714 (2010).
3. M. HIRANO, T. YONOMOTO, M. ISHIGAKI, N. WATANABE, Y. MARUYAMA, Y. SIBAMOTO, T. WATANABE, and K. MORIYAMA, J. Nucl. Sci. Technol. **49**, 1 (2012).
4. S. BRAGG-SITTON, Nucl. News. **57**, 83 (2014).
5. C.R.F. AZEVEDO, Eng. Fail. Anal. **18**, 1943 (2011).
6. L.J. OTT, K.R. ROBB, and D. WANG, J. Nucl. Mater. **448**, 520 (2014).
7. L.L. SNEAD, T. NOZAWA, Y. KATOH, T.-S. BYUN, S. KONDO, and D.A. PETTI, J. Nucl. Mater. **371**, 329 (2007).
8. M. BEN-BELGACEM, V. RICHET, K.A. TERRANI, Y. KATOH, and L.L. SNEAD, J. Nucl. Mater. **447**, 125 (2014).
9. K.G. FIELD, X. HU, K.C. LITTRELL, Y. YAMAMOTO, and L.L. SNEAD, J. Nucl. Mater. **465**, 746 (2015).
10. X. HU, K.A. TERRANI, B.D. WIRTH, and L.L. SNEAD, J. Nucl. Mater. **461**, 282 (2015).
11. D.J. PARK, H.G. KIM, J.Y. PARK, Y. IL JUNG, J.H. PARK, and Y.H. KOO, Corros. Sci. **94**, 459 (2015).
12. B.A. PINT, K.A. UNOCIC, and K.A. TERRANI, Mater. High Temp. **32**, 28 (2015).
13. H. GÖTLIND, F. LIU, J.-E. SVENSSON, M. HALVARSSON, and L.-G. JOHANSSON, Oxid. Met. **67**, 251 (2007).
14. S. KOBAYASHI and T. TAKASUGI, Scr. Mater. **63**, 1104 (2010).
15. C. CAPDEVILA, M.K. MILLER, and J. CHAO, Acta Mater. **60**, 4673 (2012).
16. Y. YAMAMOTO, B. PINT, K.A. TERRANI, K. FIELD, S. MALOY, and J. GAN, J. Nucl. Mater. **467**, 703 (2015).
17. B.A. PINT, K.A. TERRANI, M.P. BRADY, T. CHENG, and J.R. KEISER, J. Nucl. Mater. **440**, 420 (2013).
18. Z.G. ZHANG, F. GESMUNDO, P.Y. HOU, and Y. NIU, Corros. Sci. **48**, 741 (2006).
19. G. BERTHOMÉ, E. N'DAH, Y. WOUTERS, and A. GALERIE, Mater. Corros. **56**, 389 (2005).
20. R. CHEGROUNE, E. SALHI, A. CRISCI, Y. WOUTERS, and A. GALERIE, Oxid. Met. **70**, 331 (2008).
21. S. CANOVIC, J. ENGKVIST, F. LIU, H. LAI, H. GÖTLIND, K. HELLSTRÖM, J.-E. SVENSSON, L.-G. JOHANSSON, M. OLSSON, and M. HALVARSSON, J. Electrochem. Soc. **157**, C223 (2010).
22. T. CHENG, J.R. KEISER, M.P. BRADY, K.A. TERRANI, and B.A. PINT, J. Nucl. Mater. **427**, 396 (2012).
23. S.R.J. SAUNDERS, M. MONTEIRO, and F. RIZZO, Prog. Mater. Sci. **53**, 775 (2008).
24. G.J. TATLOCK, W.J. QUADAKKERS, G. BORCHARDT, I. METALLURGIE, and T. V CLAUSTHAL, Mater. High Temp. **17**, 87 (2000).
25. D.J. YOUNG, *High Temperature Oxidation and Corrosion of Metals*, pp. 1-27, T. BURSTEIN, Ed., Elsevier, Oxford, UK(2008).
26. H. BUSCAIL, S. HEINZE, and P. DUFOUR, J. Chim. Phys. **94**, 553 (1997).
27. I. GURRAPPA, S. WEINBRUCH, D. NAUMENKO, and W. J. QUADAKKERS, Mater. Corros. **51**, 224 (2000).
28. S. G. GOPALAKRISHNAN, INTERNAL OXIDES AS TEMPLATES FOR SURFACE OXIDE LAYERS WITH HIGH EMISSION COEFFICIENT AND OPTIMISED BARRIER PROPERTIES SAYEE GANESH GOPALAKRISHNAN, 2013.